CHAPTER 3

APPLICATION OF PURE ZnO AND Nb-DOPED ZnO NANOPARTICLES FOR USE AS PHOTOVOLTAIC DEVICES

Polymer photovoltaic cells are attractive sources of electrical energy because they combine flexibility with low-cost fabrication. The most efficient devices to date have been developed based on bulk-heterojunction (BHJ) systems, constructed by blending p-type conjugated polymers with n-type conjugated polymers [1–3], fullerenes [4–5], or inorganic semiconductor nanoparticles, such as TiO_2, ZnO, CdSe, and C_{60} [6–10]. Zinc oxide is a very promising metal oxide of wideband gap semiconductor for use in photovoltaic cell because of its abundance and particularly with low cost, nontoxicity, high electron mobility, low crystallization temperature, and ease of nanoparticles fabrication.

It was shown recently that ZnO can also be used as an electron acceptor to dissociate excitons formed in conjugated polymers, thus combining the advantages of organic semiconductors (flexibility, solutions processing) with those of inorganic semiconductors (stability, high mobility). Band gap engineering of ZnO has been demonstrated as an efficient way to increase open-circuit voltage and solar cell efficiency. Olson et al. [11] demonstrated the beneficial effect of band gap tuning with $Mg_xZn_{1-x}O$ in the case of hybrid solar cells using poly (3-hexylthiophene) (P3HT) as the p-type light absorber. So far, the highest efficiencies have been obtained in the

Unfortunately, the power conversion efficiencies of such hybrid polymer solar cells are too low, ~2.0% for inorganic/organic hybrid cells, for practical applications. Janssen and co-workers [12] demonstrated 1.6% efficient BHJ structures by blending 5 nm diameter ZnO nanoparticles with MEH-PPV and 0.9% efficient solar cells in blends of ZnO and P3HT. Many research groups have developed solar cells based on P3HT and conjugated fullerene composites [4, 5, 13]. Although much progress has been achieved, with several reported polymer solar cell devices providing power conversion efficiencies of 3%–6%, there remains room for improvement.

Doping Nb into ZnO is quite attractive because there is a valence difference of three between Nb^{5+} and Zn^{2+}, thus each Nb atom can contribute more than one electron to the electrical conductivity [14]. To study the device efficiency as a function of the formulation and amount of Nb-doped ZnO nanoparticles, find the optimal loading percentages for each and study the effect of Nb doping on composite solar cells using the 3.00 mol% Nb-doped ZnO nanoparticles and the use of 1, 3, 5-trichlorobenzene (TCB) as co-solvent for enhancing nanostructured P3HT:PCBM:Nb-doped ZnO layer. We synthesized highly crystalline nanoparticles of pure ZnO and ZnO doped with 0.50, 1.00, and 3.00mol% Nb by flame spray pyrolysis (FSP) technique, for specific methods of production of the nanoparticles and photovoltaic devices. It is well known that the surface characteristics of ZnO, determined by the different fabrication processes, will influence the optical properties as well as the final degradation efficiency [15]. FSP is a very promising technique for synthesis of high purity nanosized materials with the capability to control size and crystallinity. The method has been applied to prepare metal oxide-supported particles and

heterogeneous catalysts. In addition Nb is a versatile dopant and is widely applied as catalytic metal oxide [16].

3.1 Introduction

As the global energy demand continues to increase every year, the limiting supply of today's main energy sources (i.e. oil, coal, uranium) and their detrimental long-term effects on the natural balance on our planet, underscore the urgency of developing renewable energy sources. Today's plants are unable to absorb the huge amount of extra carbon dioxide that is released in the earth's atmosphere mainly by burning of fossil fuel [17–18]. As a result, the increased concentration of carbon dioxide in the atmosphere considerably adds to the greenhouse effect which will increase the global mean surface temperature [18]. The consequences of these chances are already seen by an increase in the frequency and severity of natural disasters [17]. Fortunately, we have renewable energy sources which neither run out nor have any significant harmful effects on the environment. Harvesting energy directly from the sunlight using photovoltaic (PV) technology is being widely recognized as an essential component of future global energy production. Provided that PV devices can be made truly economically competitive with fossil fuels and other emerging renewable energy technologies, large scale manufacturing of these devices offers a sustainable energy source which can supply a significant fraction of our daily energy needs.

3.1.1 Inorganic solar cells

The photovoltaic cells have become extensively studied since the 1950 when the first crystalline silicon solar cell, which had an efficiency of 6%, was developed at

Bell Laboratories [19]. Since then, the efficiency has reached 24% for crystalline Si solar cells [20], which is already close to the theoretical predicted upper limit of 30% [21]. Practically all conventional inorganic solar cells incorporate a semiconductor that is doped to form a p-n junction across which the photovoltage is generated. The p side contains an excess of the positive charges (holes), and the n side contains an excess of the negative charges (electrons). In the region near the junction an electric field is formed and the electrons and holes, which are generated through light absorption in the bulk of Si, diffuse to this junction, where they are directed by the electric field towards the proper electrode. Over the years, solar cells have been made from many other semiconductor materials with various device configurations such as single-crystal, polycrystalline, and amorphous thin-film structures. At present, crystalline Si solar cells are by far most dominant PVs used and account for more than 85% of the market.

Although in the last 5 years the production of PV modules was increased steadily by an annual average of 40%, the semiconductor PV still accounts for less that 0.1% of the total world energy production. One of the major obstacles for the market implementation of PV cells is the large production costs for Si based technology. However, despite much effort of further reducing the price, large scale production of Si-based solar cells will be limited by the availability of raw materials, such as solar-grade Si. Therefore, to ensure a sustainable technology path for PV, the development of new materials and device structures are required.

3.1.2 Organic solar cells

Organic materials bear the potential to develop a long-term technology that is economically viable for large-scale power generation based on environmentally safe

materials with unlimited availability. Organic semiconductors are a less expensive alternative to inorganic semiconductors like Si; they can have extremely high optical absorption coefficients which offer the possibility for the production of very thin solar cells. Additional attractive features of organic PVs are the possibilities for thin flexible devices which can be fabricated using high through put, low temperature approaches that employ well established printing techniques in a roll-to-roll process [22, 23]. This possibility of using flexible plastic substrates in an easily scalable high-speed printing process can reduce the balance of system cost for organic PVs, resulting in a shorter energetic pay-back time.

The electronic structure of all organic semiconductors is based on conjugated π-electrons. A conjugated organic system is made of an alternation between single and double carbon-carbon bonds. Single bonds are known as σ–bonds and are associated with localized electrons, and double bonds contain an σ–bond and a π–bond. The π–electrons are much more mobile than the σ–electrons; they can jump from site to site between carbon atoms due to the mutual overlap of π–orbitals along the conjugation path, which causes the wave functions to delocalize over the conjugated backbone. The π–bands are either empty (called the Lowest Unoccupied Molecular Orbital–LUMO) or filled with electrons (called the Highest Occupied Molecular Orbital–HOMO). The band gap of these materials ranges from 1 to 4 eV. This π–electron system has all the essential electronic features of organic materials: light absorption and emission, charge generation and transport. Figure 3.1 shows several examples of conjugated organic moieties.

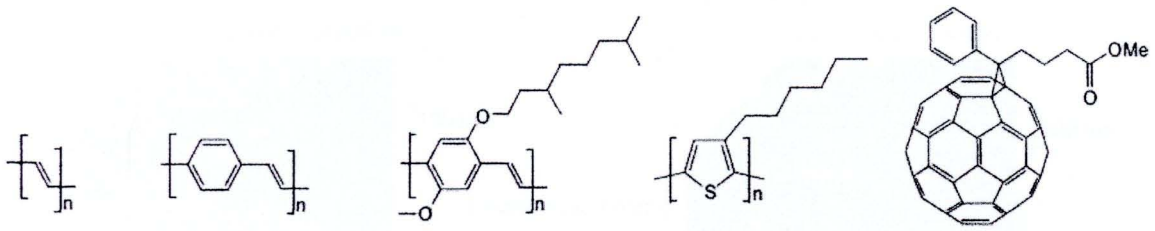

(a) PA (b) PPV (c) MDMO-PPV (d) P3HT (e) PCBM

Figure 3.1 Chemical structures and abbreviations of some conjugated organic molecules. From left: poly(acetylene) PA, poly(para-phenylene-vinylene) PPV, a substituted PPV (MDMO-PPV), poly(3-hexyl thiophene) P3HT, and a C_{60} derivative (PCBM, called PCBM throughout this chapter. In each compound one can identify a sequence of alternating single and double bonds.

A typical organic PV cell consists of a photoactive layer sandwiched between two different electrodes, one of which should be transparent in order to allow the incoming photons to reach the photoactive layer, as seen in Figure 3.2. This photoactive layer is based on a single, a bi-layer, or a mixture of two (or more) components. Upon light absorption the charge carriers are generated inside the photoactive layer and due to the presence of an electric field, provided by the asymmetrical ionization energies/work functions of the electrodes (anode and cathode), these charges are transported and collected into the external circuit. In this way an organic solar cell converts light into electricity.

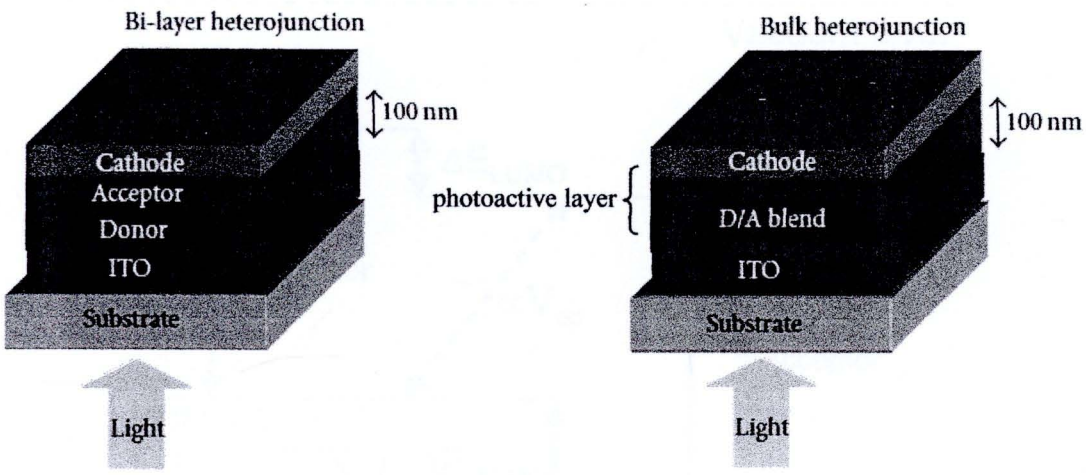

Direct path for charge carriers to electrodes

(a)

Large interfacial area due to phase separation in the blend, but percolation needed

(b)

Figure 3.2 Schematic layout of an organic solar cell.

Figure 3.3 shows a schematic drawing of the energy levels in an organic solar cell. The maximum short-circuit current is determined by the smaller optical band gap of the two materials, and V_{OC} is proportional to the difference between the HOMO level of the donor material and the LUMO level of the acceptor compound. In a conjugated polymer - [6,6]–phenyl C_{61}-butyric acid methyl ester (PCBM) solar cell system, the value of V_{OC} can be estimated from the energy difference between HOMO of the donor and LUMO of the PCBM, using the following equation [24].

$$V_{OC} = (1/e)(|E^{Donor}HOMO| - |E^{PCBM}HOMO|) - 0.3V \tag{3.1}$$

where e is the elementary charge. For P3HT-PCBM solar cells, the energy difference between the HOMO of the P3HT and the LUMO of the PCBM is 1.03 eV; therefore, we predicted that the value of V_{OC} would be 0.73 V.

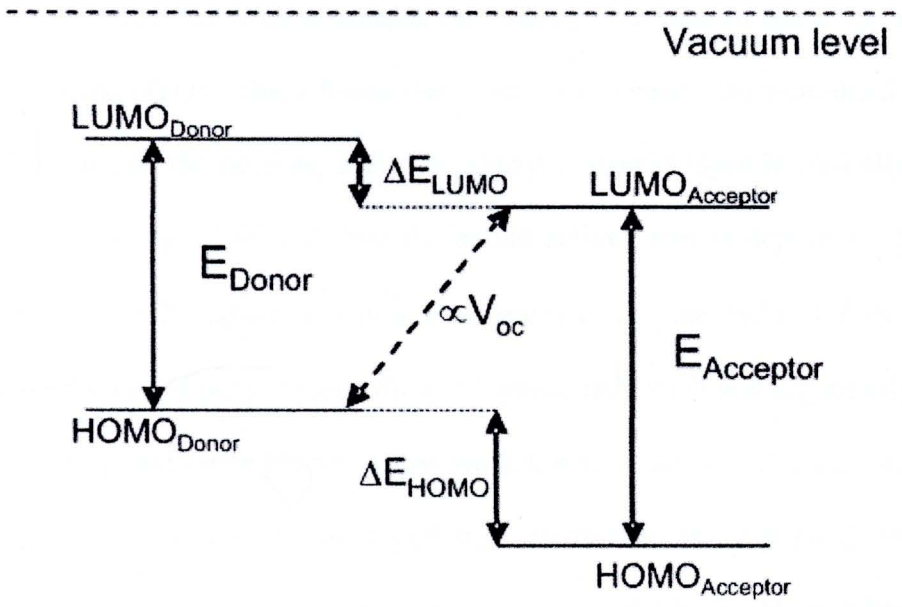

Figure 3.3 Schematic drawing of the donor and acceptor energy levels.

3.1.3 Advantages of organic solar cells

Scientists and engineers are looking for new materials and systems. Organic semiconductors, including conjugated polymers, are promising materials for solar cells. They are cheap in production and purification. Furthermore, organic chemistry can tailor the materials for the demand. Organic devices are flexible, lightweight and ease of production [25]. Polymer procession is done by spin casting [26], doctor blading [27–28] has been successfully applied for solar cells preparation, ink-jet printing or of even roll-to-roll processing are well known techniques for polymer processing and could be principally used for device fabrication. All these techniques are performed at room temperature.

3.1.4 Characterization of organic bulk heterojunction solar cells

Bulk heterojunction solar cells with a photoactive layer prepared from a conjugated polymer and fullerene molecules, are fabricated by depositing (i.e. spin

coating) the active layer from a solution on a transparent bottom electrode, normally indium-tin-oxide (ITO), which forms the anode. To enhance the reproducibility and the performance of the devices, a thin conductive organic layer is typically applied from solution on top of ITO, before the actual active layer is deposited. The most widely used cover layer on ITO is a transparent composite PEDOT:PSS [29–31], consisting of oxidized polyethylene dioxythiophene (PEDOT) and impartially anionic form polystyrene sulfonate (PSS). A low work function metal (calcium, barium, or a thin layer of lithium fluoride; all toped with aluminum) is evaporated under high vacuum on top of the photoactive layer and serves as cathode, as shown schematically in Figure 3.4(a). In order to investigate the PV performance of a cell, as well as its electric behavior, the current density-voltage (J-V) characteristics in the dark and under illumination are considered.

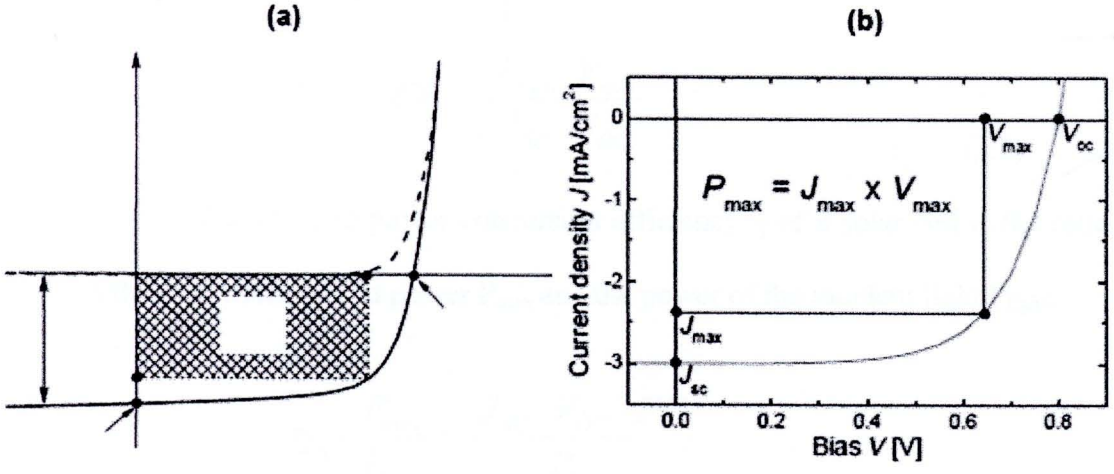

Figure 3.4 Typical J-V characteristics of an organic PV cell (a) in the dark (dashed line) and illumination (solid line) conditions (b) J_{SC} and V_{OC} are shown. The maximum output power (P_{max}) is given by the rectangle $J_{max} \times V_{max}$.

Figure 3.4(b) shows a typical J-V curve of a PV device in the dark (dashed line) and under illumination (solid line). When the cell is illuminated, the J-V curve is shifted down by the amount of photocurrent (J_{ph}) generated. The open-circuit voltage, V_{OC}, is the maximum photovoltage that can be generated in the cell and corresponds to the voltage where current under illumination is zero. The maximum current that can run through the cell at zero applied voltage is called the short-circuit current, J_{SC}. The maximum of the obtained electrical power P_{max} is located in the fourth quadrant where the product of current density J and voltage V reached its maximum value ($J_{max} \times V_{max}$; as seen in Figure 3.4(b)). It is observed from the Figure 3.4(b) that P_{max} is bigger when the J-V curve resembles a rectangular with the area $J_{SC} \times V_{OC}$. The ratio between (the rectangle of) P_{max} and the product of (or a rectangle defined by) J_{SC} and V_{OC} measure the quality of the shape of the J-V characteristics, and are defined as the fill factor (FF):

$$FF = \frac{J_{max} \cdot V_{max}}{J_{SC} \cdot V_{OC}} \tag{3.2}$$

Thus $P_{max}=J_{SC} \cdot V_{OC} \cdot FF$. The power conversion efficiency η of a solar cell is the ratio between the maximum output power P_{max} and the power of the incident light P_{light}:

$$\eta = \frac{P_{max}}{P_{light}} = \frac{J_{SC} \cdot V_{OC} \cdot FF}{P_{light}} \tag{3.3}$$

$$\eta_{pc} = \frac{P_{max}}{P_{light}} = \frac{J_{SC} \cdot V_{OC} \cdot FF}{P_{light}} \times 100 \tag{3.4}$$

Because of the wavelength and intensity dependence of P_{max}, the power conversion efficiency η should be measured under standard test conditions. Equation 3.2 shows

that in order to increase η, for the same incident light power P_{light}, either J_{SC}, V_{OC}, or FF (or all) need to be increased. For organic solar cells based on polymer:fullerene bulk heterojunctions, the magnitude of J_{SC}, V_{OC}, and FF depends on parameters such as: light intensity [32], temperature [33–34], composition of the components [35], thickness of the active layer [36], the choice of electrodes used, as well as the solid state morphology of the film [37]. The power conversion efficiency (η_{pc} in %) is defined as the ratio of P_{max} and P_{light}.

Apart from η_{pc}, the incident photon to current conversion efficiency (IPCE), also known as the external quantum efficiency (EQE), is often used. The IPCE compares the number of charge carriers collected at zero bias (J_{SC}) to the number of incident monochromatic photons. Measuring the IPCE at different wavelengths results in a spectral response of the solar cell. Because the short-circuit current density (J_{SC}) not necessarily increases linearly with P_{light}, the absolute IPCE-values generally depend on the P_{light} of the monochromatic light [38]. The same, of course, holds for η_{pc}. Again, this explains the necessity for both η_{pc} and IPCE measurements under appropriate standard test conditions. This means that apart from the monochromatic light, continuous irradiation under standard test conditions is required for meaningful comparison of IPCE spectra [39]. Another characteristic value is the internal quantum efficiency (IQE). The IQE is the ratio of the number of charge carriers collected at zero bias (J_{SC}) and the number of actually absorbed monochromatic photons. The IQE gives insight on the efficiency of the charge generation, transport, and collection processes. At a given wavelength λ, the product of the absorption A and IQE equals IPCE as in Equation (3.5).

$$IPCE(\lambda) = EQE(\lambda) = A(\lambda) \times IQE(\lambda) = \frac{1.24 \times 10^5 \times J_{SC}(\lambda)}{P_{light} \times \lambda} \quad (3.5)$$

The incident photon to current conversion efficiency (IPCE in %) or external quantum efficiency (EQE) is the product of the absorption of the photoactive layer (A) and the internal quantum efficiency (IQE) with Jsc, P_{light}, and the wavelength λ in mA/cm^2, mW/cm^2, and nm, respectively.

3.1.5 Principles of Bulk Heterojunction Solar Cells

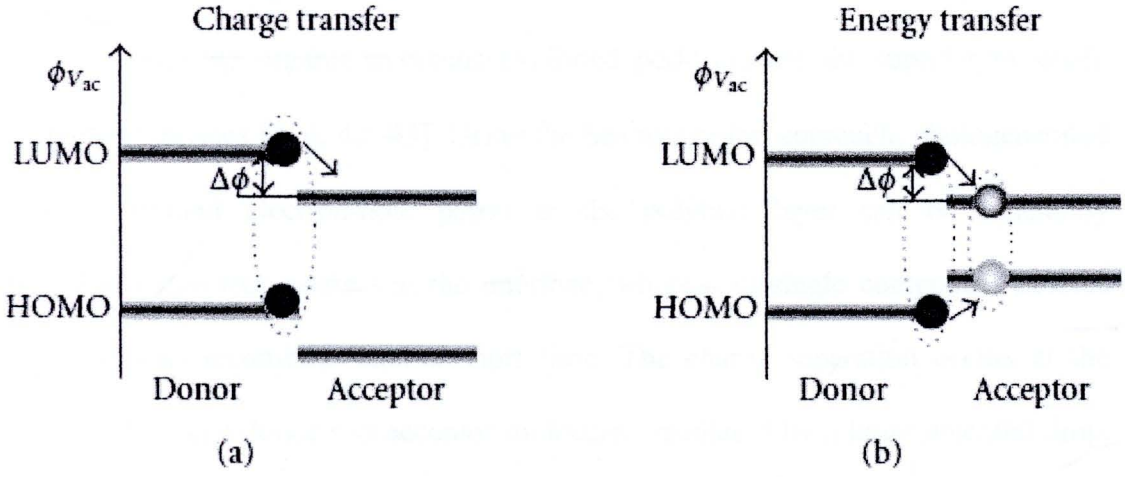

Figure 3.5 The interface between two different semiconducting polymers (D = donor, A = acceptor) can facilitate either charge transfer by splitting the exciton or energy transfer, where the whole exciton is transferred from the donor to the acceptor.

Three steps are essential for the conversion of light into electricity, how it is done by solar cells [40]:

- absorption of light,
- charge carrier generation
- selective transport of the opposite charges to the opposite contacts

Light with an energy $h\upsilon \geq$ the band gap E_g can excite electrons over the bandgap from the valence band to the conduction band. In conjugated polymer, this excitations are the HOMO-LUMO [41] excitations. These excited electrons can be converted to current. Hence, the amount of absorbed light is directly related to the short circuit current. Absorption spectrum and thickness of the active layer are the important parameter. The thickness cannot be increased over a certain limit because of the limited mobility of the charge carriers.

The most important discovery on the route to high efficiency organic solar cells was the finding that solar cells containing a heterojunction between hole and electron accepting organic materials exhibited performances far superior to single component devices [3, 4, 42–43]. Using the heterojunction approach, photogenerated excitons (bound electron-hole pairs) in the polymer layer can be efficiently dissociated into free carriers at the interface, whereas in single component devices most excitons recombine after a short time. The charge separation occurs at the interface between donor and acceptor molecules, mediated by a large potential drop. After photo-excitation of an electron from the HOMO to the LUMO, the electron can jump from the LUMO of the donor (the material with the higher LUMO) to the LUMO of the acceptor if the potential difference $\Delta\Phi$ between the ionization potential of the donor and the electron affinity of the acceptor is larger than the exciton binding energy as shown in Figure 3.5. However, this process, which is called photoinduced charge transfer, can lead to free charges only if the hole remains on the donor due to its higher HOMO level. In contrast, if the HOMO of the acceptor is higher, the exciton transfers itself completely to the material of lower-band gap accompanied by energy loss.

The ultrafast charge transfer is a good biomimetic model for the primary photoexcitation in green plants. Whereas in photosynthesis the light energy is converted into chemical energy, solar cells are intended for the generation of electricity.

In the third step, the created charges have to be transported selectively to the contacts. The holes are transported by the polymer to the ITO contact and the electrons to the Al. Conjugated polymers show high mobilities along the chains, but the mobility is limited by the hopping between the chains. The electrons are transported by the fullerene via a hopping process. The most efficient charge separation is found for a cell containing 80% fullerene [40, 43]. Similar values are found for polymer solar cells with perylene acceptors [44–45]. For charge generation, a few percent would be sufficient. But the interconnection of all acceptor molecules in the bulk is of importance for efficient charge collection. Isolated fullerene molecules or clusters are charge traps and the electrons are captivated there.

3.1.6 Literature review

Solution-processed bulk-heterojunction photovoltaic cells were first reported in 1995 [4]. It took another 3–4 years until the scientific community realized the huge potential of this technology, and suddenly, in 1999, the number of publications in that field started to rise exponentially. Since then, the number of publications on organic semiconductor photovoltaics has increased by about 65% per year.

Summary of reports focusing on photovoltaic devices based on P3HT:PCBM and P3HT:PCBM:metal or metal oxice blends are shown in Table 3.1.

Table 3.1 Nonexhaustive survey of reports focusing on photovoltaic devices based on P3HT:PCBM and P3HT:PCBM:Metal or Metal Oxice blends.

Year/Ref.	Donor	M_w [g mol^{-1}]	Ratio to PCBM (weight)	Metal or Metal Oxice	Layer thickness [nm]	Solvent	Annealing time [min]	Annealing Temp. [°C]	Max EQE [%]	V_{oc} [V]	FF	Jsc [mA cm^{-2}]	Eff [%]	Light intensity [mW cm^{-2}]
2003 [44]	-	-	-	-	110	DCB	4	75	70	0.55	0.6	8.5	3.5	80
2004 [45]	P3HT(Rieke)	-	1:2	-	350	CB	4	75	65	0.54	0.37	15.2	3.1	100
2005 [46]	P3HT(Merck)	11 600	1:1	-	-	CB	15	140	58	0.61	0.53	9.4	3.0	100
2005 [47]	P3HT(Rieke)	-	1:1	-	220	DCB	10	110	63	0.61	0.67	10.6	4.4	100
2005 [52]	MDMO-PPV	-	-	ZnO NPs 30 vol%	100	CB	-	-	-	0.81	0.59	2.4	1.6	100
2006 [48]	P3HT(Merck)	21 100	1:1	-	175	CB	120	140	70	0.6	0.52	12	4.4	85
2007 [51]	P3HT(Rieke)	-	1:0.6	ZnO nanorod	-	CB	-	-	58	0.57	0.50	9.6	2.7	100
2007 [58]	P3HT(Rieke)	~ 48 000	1:0.6	-	500	CB	8	158	~ 60	-	-	-	6.1	100
2008 [49]	P3HT(Rieke)	-	1:1	-	220	DCB	10	120	87	0.64	0.69	11.3	5.0	100
2008 [52]	P3HT 10 mg/mL	-	-	ZnO/PDI 100/1 mg/mL	-	CF/MT	60	160	-	0.35	-	9.55	-	100
2009 [50]	-	38 000	1:1	0.04 wt% Pt	80	CF	5	110	-	0.64	0.62	10.0	4.08	100

Efficiencies of organic solar cells based on an interpenetrating network of a conjugated polymer and a fullerene as donor and acceptor materials still need to be improved for commercial use. Padinger et al. [44] have developed a postproduction treatment that improves the performance of solar cells based on P3HT and PCBM by means of a tempering cycle at elevated temperatures in which an external voltage is simultaneously applied, resulting in a significant increase of the short-circuit current. Using this postproduction treatment, an enhancement of the short-circuit current density, J_{SC}, to 8.5 mA/cm^2 under illumination with white light at an illumination intensity of 800 W/m^2 and an increase in external quantum efficiency (IPCE, incident photon to collected electron efficiency) to 70% are demonstrated.

The photovoltaic properties of polymer-fullerene bulk-heterojunction solar cells with light absorbers based on the conjugated polymers P3HT, blended with the acceptor-type methanofullerene PCBM, are discussed by Riedel et al. [45]. The results showed that active layer thickness could be increased resulting in high values of short-circuit current due to improved light absorption. A large increase of the absorber thickness results in a large photocurrent of J_{SC} = 15.2 mA/cm^2 due to higher absorption. This value was by nearly 7 mA/cm^2 higher than the value obtained for devices with a 100 nm thick active layer. The open-circuit voltage measured was 0.54 V. The fill factor of the L = 350 nm device was reduced to 37%, as compared to 50%-60% for 100 nm samples. The power conversion efficiency of 3.1% (P_{Light} = 100 mW/cm^2, T = 300 K) was obtained.

Kim et al. [46] reported enhanced efficiency bulk heterojunction organic solar cells using blend films of regioregular P3HT and PCBM that were subjected to a thermal annealing process. Blend films (P3HT:PCBM = 1:1 by weight) were prepared

using chlorobenzene and 1, 2-dichlorobenzene in order to investigate the role of the solvent. Irrespective of the chosen solvent, the optimal device annealing temperature was found to be 140°C. The highest power conversion efficiency, 3% under air mass 1.5 simulated solar illumination (100 mW/cm^2), was achieved by device annealing at 140°C for 15 min using blend films prepared from chlorobenzene (2.3% for 1, 2-dichlorobenzene).

Li et al. [47] reported highly efficient polymer solar cells based on a bulk heterojunction of polymer P3HT and PCBM. Controlling the active layer growth rate results in an increased hole mobility and balanced charge transport. Together with increased absorption in the active layer, this results in much-improved device performance, particularly in external quantum efficiency. The power-conversion efficiency of 4.4% was achieved.

Kim et al. [48] studied the influence of polymer regioregularity (RR) on the molecular nanostructure, and hence on the resulting material properties and device performance. They found a strong influence of RR (95.4%) after optimizing film thickness (~175 nm) and device annealing conditions on solar-cell performance, which can be attributed to enhanced optical absorption and transport resulting from the organization of P3HT chains and domains. Further optimization of devices using the highest RR material resulted in a power conversion efficiency of 4.4% and 68–73% EQE (450–550 nm).

To minimize interfacial power losses, thin (5−80 nm) layers of NiO, a p-type oxide semiconductor, are inserted between the active organic layer, P3HT + PCBM, and the ITO anode of bulk-heterojunction ITO/P3HT:PCBM/LiF/Al solar cells were studied by Irwin et al. [49]. The interfacial NiO layer was deposited by pulsed laser deposition directly onto cleaned ITO, and the active layer was subsequently deposited

by spin-coating. Insertion of the NiO layer afforded cell power conversion efficiencies as high as 5.2% and enhanced the fill factor to 69% and the open-circuit voltage (V_{OC}) to 638 mV versus an ITO/P3HT:PCBM/LiF/Al control device. The value of such hole-transporting/electron-blocking interfacial layers is clearly demonstrated and should be applicable to other organic photovoltaics.

Chang et al. [50] prepared polymer solar cells incorporating an active layer of P3HT:PCBM blended with platinum nanoparticles (Pt NPs). The results showed that after blending a small amount 0.04 wt% of Pt NPs into the P3HT:PCBM active layer, a power conversion efficiency of 4.08%, a 55% improvement over that of the unmodified polymer solar cell (AM1.5G = 2.63%) was obtained. The values of J_{SC} increases from 8 to 10 mA/cm^2 and the FF increases from 0.51 to 0.62.

Photovoltaic performance of the hybrid devices consisting of polymer/fullerene/ZnO nanorod array was studied by Takanezawa et al. [51]. The dependence of the photovoltaic performance on the ZnO nanorod length and the organic layer thickness was investigated, and it was concluded that the ZnO nanorod array plays an important role in collecting photogenerated electrons and acts as a conducting path to the indium tin oxide electrode. Fill factor of the devices increased from 38% to 50% when the array of the ZnO nanorods was introduced, which directly contributed to the improvement of the power conversion efficiencies up to 2.7%. As the peak absorption of the device reaches >97% in a transmitting geometry, the results shown here gave the insights toward designing the devices with efficient utilization of the incident light.

Bulk heterojunction photovoltaic devices based on blends of a conjugated polymer poly[2-methoxy-5-(3′,7′-dimethyloctyloxy)–1,4-phenylenevinylene]

(MDMO-PPV) as electron donor and crystalline ZnO nanoparticles (*nc*-ZnO) as electron acceptor was studied by Beek et al. [52]. It was found that the performance of the *nc*-ZnO: MDMO-PPV solar cells depend on the concentration of ZnO and the thickness of the active layer. The best performance was found for a blend with 30 vol% ZnO and thickness of 100 nm, sandwiched between a transparent (PEDOT:PSS on ITO) and a metal (aluminum) electrode. These devices provide a photovoltaic effect with an estimated efficiency of about 1.6%.

A soluble perylene-derivative dye, N, N'-didodecyl-3, 4, 9, 10-perylene tetracarboxylic dimide (PDI) was used to enhance the photoelectric efficiency of the hybrid P3HT/ZnO bulk-heterojunction solar cells as reported by Wang et al. [53]. ZnO nanoparticles were synthesized using the method reported by Beek et al. [52]. Solar cells were prepared by sandwiching the spin-coating composite films between PEDOT:PSS covered ITO glasses and aluminum electrodes. PDI could absorb the sunlight in a broad wavelength range. By blending with PDI, the light absorption and exciton separation of the P3HT/ZnO solar cells could be significantly improved. The photocurrent under white light could be increased from 6.35 to 9.55 mA/cm^2.

Hybrid polymer-metal oxide bulk-heterojunction solar cells were constructed by Janssen et al. [12]. The active layer of this device was fabricated by blending nanocrystalline zinc oxide nanoparticles prepared by hydrolysis and condensation method and P3HT. Thermal annealing of the spin-cast films and appropriate amount of ZnO in the blend significantly improved the solar-energy conversion efficiency of these hybrid solar cells to $\approx$ 0.9% under Air Mass (AM) 1.5 conditions.

The processes of charge separation and transport in hybrid bulk heterojunction solar cells using cadmium sulfide nanocrystals and the conjugated polymer poly (2-

methoxy, 5-(2'-ethyl)-hexyloxy-*p*-phenylenevinylene) as active layer were investigated by Greenham et al. [54]. It was found that phase segregation of these photovoltaic devices using the composite was crucial in providing paths for both electrons and holes to travel to the appropriate electrode without recombination. The use of nanocrystals allowed great flexibility in controlling the performance of photovoltaic devices, since both the electronic energy levels and the morphology of the composite materials may be altered by changing the nanocrystal size, concentration, and surface ligand. The energy conversion efficiency of these devices was 0.2% under Air Mass (AM) 1.5 conditions that was a typical solar spectrum.

The new architecture for high-efficiency polymer photovoltaic cells using solution-based titanium oxides as an optical spacer, P3HT-PCBM as active layer on ITO-coated glass was reported by Kim et al. [55]. An optical spacer was inserted between the active layer and the reflective electrode resulted in a redistribution of the optical electric field. The TiO_x precursor solution was spin-cast in air on top of the polymer: fullerene composite layer with a thickness of around 30 nm. The typical XRD peaks of the anatase crystalline form appeared only after sintering the spin-cast films at 500°C for 2h. The conventional device (without the TiO_x layer) showed a typical photovoltaic response with device performance. The J_{SC} was 8.4 mA/cm^2, the V_{OC} was 0.60 V, and FF was 0.40. These values corresponded to a power conversion efficiency of 8.1%. For the device with the TiO_x layer, the results demonstrated substantially improved device performance; J_{SC} increaseed to 11.8 mA/cm^2, the FF increased slightly to 0.45, while V_{OC} remained at 0.60 V. The corresponding power-conversion efficiency was 12.6%, which corresponded to an approximately 50% increase in the device efficiency.

3.2 Chemicals and equipments

3.2.1 Solar cell preparation

- Pure ZnO and Nb-doped ZnO nanoparticles
- Deionize water
- 1-butanol (Aldrich, 99.9% CAS No 71-36-3, USA)
- Regioregular Poly(3-hexylthiophene-2-5-diyl) (Rieke Metal, USA)
- [6, 6]-phenyl-C61-butyric Acid Methyl Ester (American Dye Source; USA)
- Chorobenzene (Aldrich, 99.8%, CAS No. 108-90-7, USA)
- Dimethyl Sulfoxide (BDE, 99.9%, CAS No. 67-68-5, USA)
- 3, 4-polyethylenedioxythiophene-polystyrenesulfonate (H.C.Starck, USA)
- Glass microfibre filters (Whatmann, GF/D, 2.7 μm pore size, USA)
- PTFE microfibre filters (VWR, 1 μm pore size, USA)
- PVDF microfibre filters (Millex, 0.45 μm pore size, USA)
- Syring (Becton Dickinson, 10 ml, Singapore)
- Syring (Norm-Ject, 1 ml, Germany)
- Balance (Metter Toledo, USA)
- Magnetic stirrler bar (VWR, USA)
- Hot plate stirrer (Corning, USA)
- Multi-magnestir (Lab-Line instruments, USA)
- Ultrasonic bath (Branson, USA)
- Vacuum oven (Cole-Parmer, USA)
- Ultra-violet ozone cleaning (UVOCS, USA)
- Spin coater (Specialty Coating System, P6700 series, USA)

- Evapolator (Senton Vacuum, USA)
- Power supplied (Nemic-Lambda, USA)
- Thickness monitors (Maxtek, TM-400, USA)
- Glove box (Vacuum Atmospheres Company, USA)
- ITO glass (Delta technologies, USA)
- 1, 3, 5- Trichlorobenzene (Aldrich, USA)

3.2.2 Solar cell characterization

- UV-vis absorption spectra test
- External quantum efficiency test
  - Motorized 1/4m monochromator (New port, Oriel Instruments, USA)
  - Input power (New port, Oriel Instruments, USA)
  - Power supply (New port, Oriel Instruments, USA)
- I-V characteristic test
  - Lamp power (Driel Instruments, 50–500 W, USA)
  - Lethai Voltages (Keithley, USA)
- Atomic force microscope (Nano Scope IIIa, Veeco Digital instrument)

3.3 Experimental

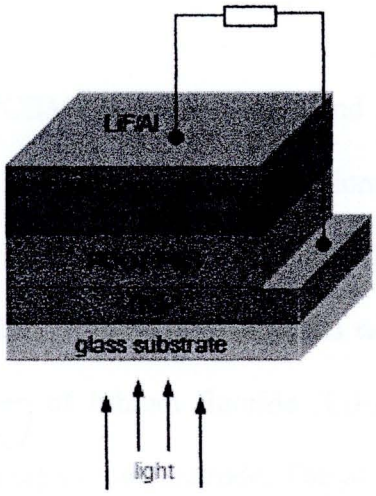

Figure 3.6 Device configuration of the polymer solar cells.

3.3.1 Device fabrication

3.3.1.1 The effect of Nb loading on the solar efficiency of the P3HT:PCBM:Nb-doped ZnO blend films and the amount of Nb-doped ZnO loading on the solar efficiency of the P3HT:PCBM:Nb-doped ZnO blend films

Devices were prepared incorporating regioregular P3HT (Rieke Metals; M_w 48,000 g mol^{-1}) and PCBM (99.5% purity) blends (both with and without added Nb-doped ZnO solution) as a donor/acceptor bulk heterojunction active layer. The polymer solar cells had the device configuration (Figure 3.6) using ITO patterned glass substrates (Delta Technologies R_s =10 Ω sq^{-1}). The substrates were cleaned in an ultrasonic bath with, deionized (DI) water, acetone and isopropyl alcohol, and then dried under vacuum in an oven. The substrate was treated with oxygen plasma for 90 min. Poly(3,4-ethylenedioxythiophene): poly(styrenesulfonate) (PEDOT:PSS) (Baytron P) was deposited onto the ITO glass substrate by spin coating at 4000 rpm and dried at 100°C for 25 min. The ZnO nanoparticles (pure ZnO, 0.50, 1.00 and 3.00

mol% Nb-doped ZnO) were prepared in 1-butanol to give the concentration of 15 mg mL^{-1}.

Four sets of P3HT:PCBM:Nb-doped ZnO blend solutions were prepared by adding Nb/ZnO solution (31 vol%) to the stirred solutions of P3HT:PCBM (1:0.7) in chlorobenzene (1 ml). The P3HT:PCBM:Nb-doped ZnO solution blend was coated on top of the PEDOT:PSS film. Finally, the substrates were transferred to a vacuum chamber to evaporate 1.5 nm of lithium fluoride (LiF) (Aldrich) and 100 nm of aluminum (Al) (Sigma-Aldrich) as top electrode. The active area of these devices is 0.38 +/- .04 cm^2. After completion, the devices were annealed for 3 min at 150°C in the glove box.

3.3.1.2 The effect of niobium doping on composite solar cells using the 3 mol% Nb-doped ZnO NPs and the use of 1, 3, 5-trichlorobenzene (TCB) as co-solvent for enhancing nanostructured P3HT:PCBM:Nb/ZnO layer

For this study, three sets of devices were fabricated. The 3.00 mol% Nb-doped ZnO nanoparticles were prepared in 1-butanol to give the concentration of 15 mg/mL. ITO patterned glass substrates. An PEDOT:PSS film was spin coated onto the ITO glass substrate, which was then dried in vacuum oven at 100°C for 25 min. 15 mg of P3HT was dissolved in 1 ml of chlorobenzene and blended with PCBM in the ratio of 1:0.7 polymer to PCBM by weight. The composite materials were spin coated onto the PEDOT:PSS layer at 1500 rpm. Lithium fluoride (LiF) and aluminum (Al) electrodes were deposited via thermal evaporation at approximately 15 nm and 100 nm thick, respectively. The active area of these devices is 0.38 +/- .04 cm^2.

For device set 1, D1 and D2 were annealed for 5 and 7 min respectively. For device set 2, D3 and D4 were prepared by adding 30 vol% of 3 mol% Nb-doped ZnO solution to P3HT:PCBM solution and annealed for 5 and 7 min respectively. Finally, device set 3, D5 and D6 were prepared by adding 30 vol% of 3.00 mol% Nb-doped ZnO solution and 1, 3, 5-trichlorobenzene (TCB) (3.5 mg) to P3HT:PCBM solution and annealed for 5 and 7 min respectively.

3.3.2 Measurements and characterization

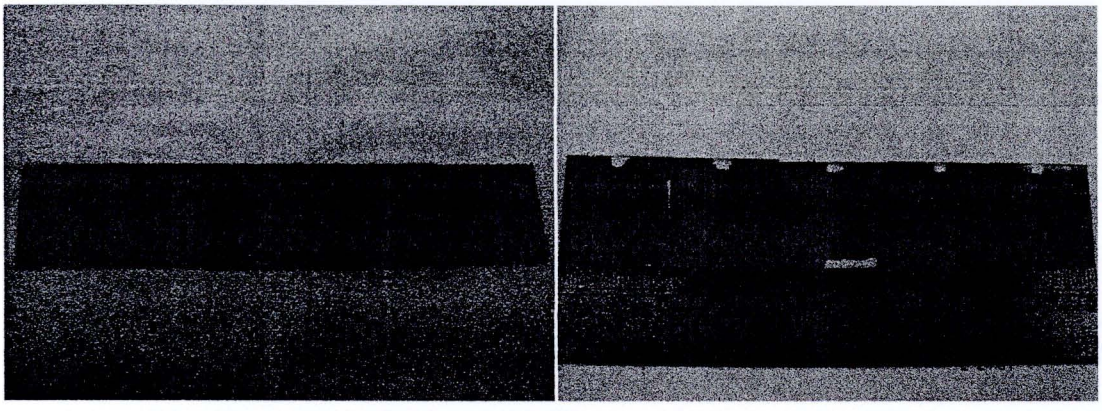

(a) **(b)**

Figure 3.7 The bulk heterojunction photovoltaic devices (a) before and (b) after depositing with LiF and Al electrode.

The Current-voltage (J-V) characteristics of the photovoltaic cells were tested in air at room temperature (298 K) using a Keithley 2400 source measurement unit, and an Oriel filter was Xenon lamp (150W) coupled with an AM1.5 filter was used as the light source. The light intensity was 120 mW/cm^2 and 100 mW/cm^2 on the sample surfaces measured by a photodetector.

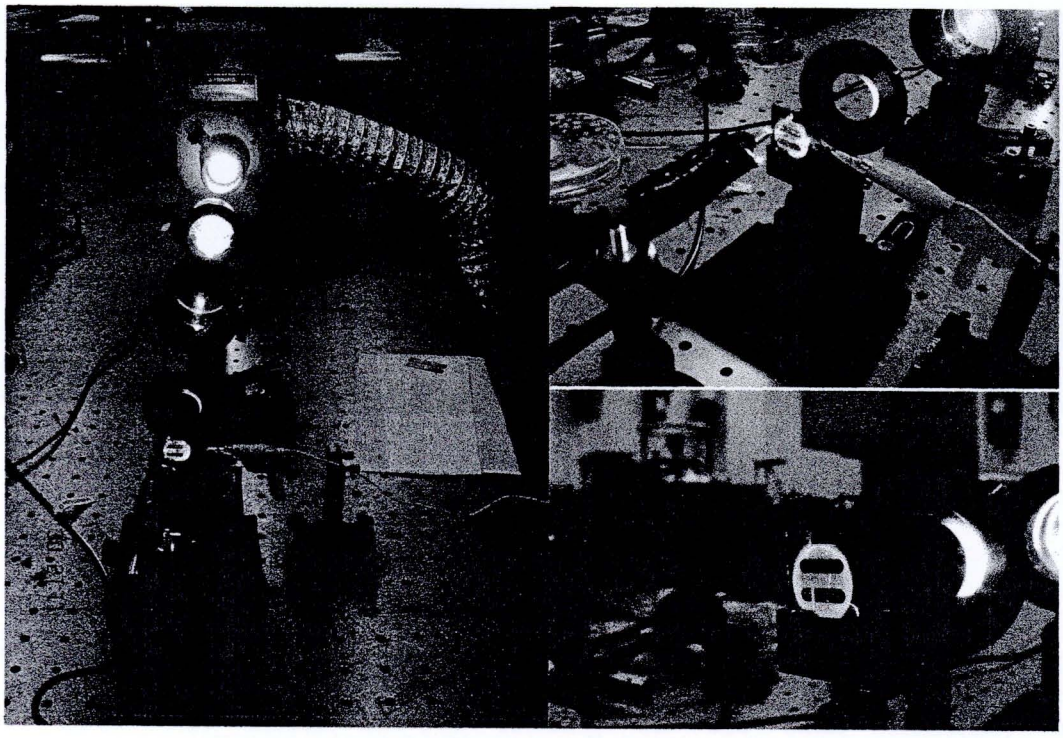

Figure 3.8 The solar simulation system.

UV-vis spectra of the spin-coated films were recorded on a Perking-Elmer Lambda Bio-40 spectrophotometer. External Quantum Efficiency (EQE) measurements were performed using a Hitachi F-4500 fluorescence spectrophotometer with an AM 1.5 filter. Light intensity was adjusted in the wavelength range of 300–700 nm. All electrical measurements were performed in the air. The active area of the device irradiated by the light was defined by photo mask as 0.03 cm^2. The surface morphological features of the films were examined using atomic force microscope (AFM) system.

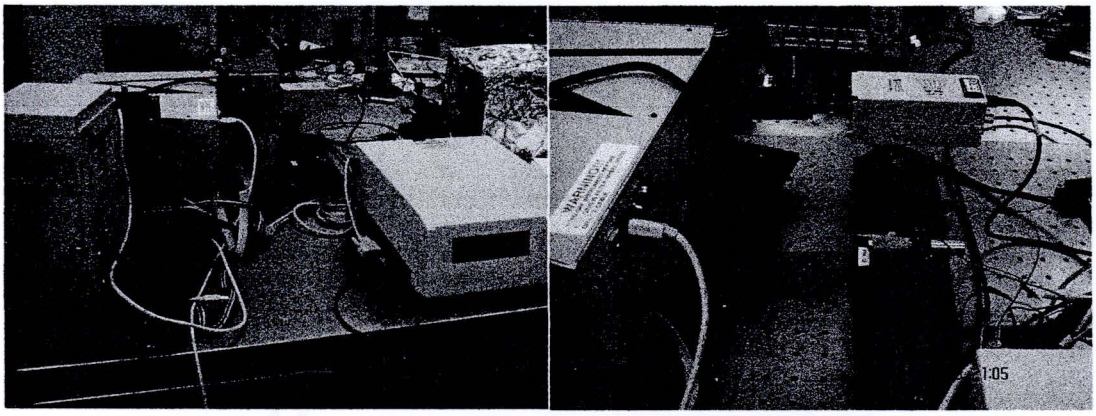

Figure 3.9 The EQE simulation system.

3.4 Results and Discussion

3.4.1 The effect of Nb loading on the solar efficiency of theP3HT:PCBM:Nb-doped ZnO blend films and the amount of Nb-doped ZnO loading on the solar efficiency of the P3HT:PCBM:Nb-doped ZnO blend films

The device structure and energy levels of the materials used in this work are shown in Figure 3.10 Excitons are formed when P3HT absorbs photons. These excitons can be disassociated at the phenyl-C61-butyric acid methyl ester (PCBM) and/or Nb-doped ZnO interfaces. ZnO and PCBM both can act as electron acceptor. ZnO has a high electron mobility [56], which can help charge-carrier collection and transport. The electrons at the lowest unoccupied molecular orbital level of PCBM (3.7 eV) can be easily transferred to the conduction band of ZnO (4.4 eV) (Figure 3.10).

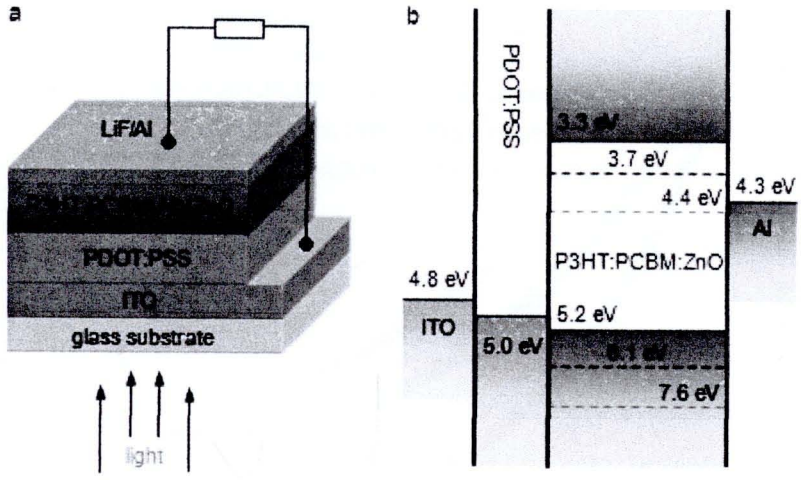

Figure 3.10 Device structure and energy level diagram of the components. (a) Schematic device structure for P3HT:PCBM BHJ photovoltaic cells with ZnO nanoparticles. (b) Energy level diagram of the components of the device (relative to vacuum level).

We investigated the effect of niobium doping on both the ZnO nanoparticles and on composite solar cells made using the Nb-doped ZnO nanoparticles. As shown in the experimental, increasing the amount of niobium used when synthesizing the ZnO nanoparticles resulted in smaller particles with more surface area. The P3HT:PCBM solution was doped with 31% by volume of Nb-doped ZnO in 1-butanol as well as ZnO nanoparticles without niobium doping. As the niobium doping percentage increased, there was an increase in the filling factor (FF) over a standard P3HT:PCBM device. There was also an increase in J_{SC} (Table 3.2). The J-V measurements and the EQE measurements were shown in Figures 3.11 and 3.12.

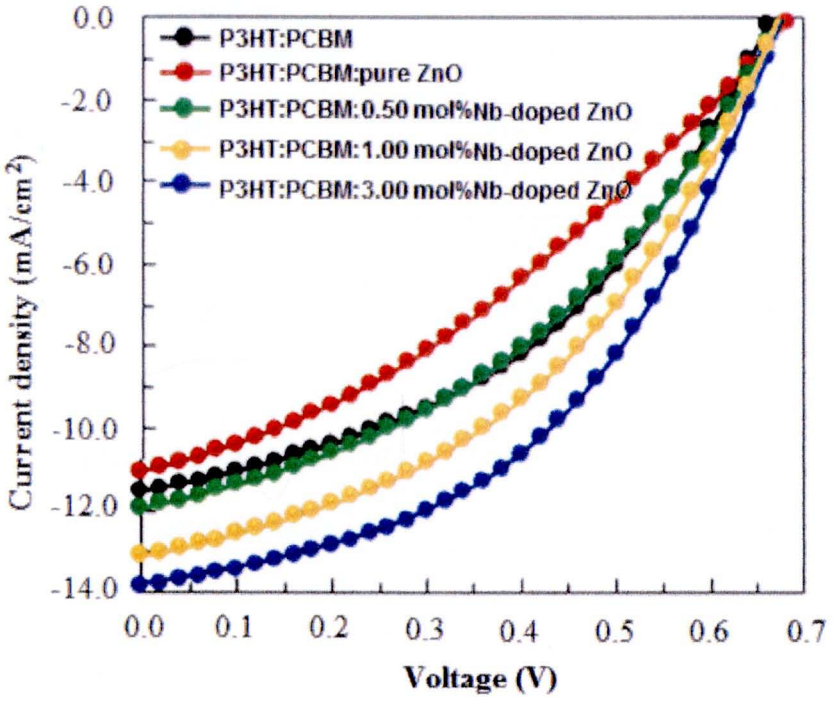

Figure 3.11 J-V curves under 120 mW/cm^2 white light illumination of Nb-doped ZnO loading with different Nb concentrations on device performance.

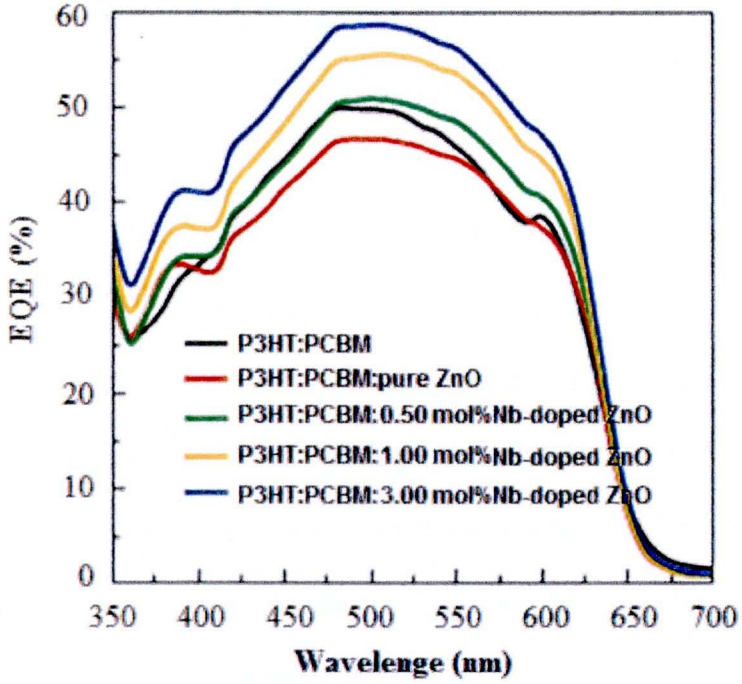

Figure 3.12 EQE spectra of Nb-doped ZnO loading with different Nb concentrations on device performance.

Table 3.2 Solar cell parameters.

Samples	V_{OC} (V)	J_{SC} (mA/cm^2)	FF	η (%)
P3HT:PCBM	0.663	11.5	0.429	2.85
P3HT:PCBM:pureZnO	0.682	11.0	0.338	2.21
P3HT:PCBM:0.50 mol% Nb-doped ZnO	0.673	11.9	0.398	2.78
P3HT:PCBM:1.00 mol% Nb-doped ZnO	0.672	13.1	0.424	3.24
P3HT:PCBM:3.00 mol% Nb-doped ZnO	0.675	13.8	0.462	3.73

Nb-doped ZnO particles synthesized with 3.00 mol% concentration of Nb were then used to investigate the effect of different loadings of nanoparticles on the photovoltaic characteristics of devices (illuminated at 120 mW/cm^2). Again, there was a small increase in open circuit voltage (V_{OC}) for Nb-doped ZnO doped devices. The Nb-doped ZnO solution-blended P3HT:PCBM films exhibited higher values of J_{SC} with the maximum value 13.9 mA/cm^2 obtained for the 30 vol% Nb-doped ZnO system (11.5 mA/cm^2 for the unmodified device), although this started to decrease at the 33 vol% loading. The increased Jsc and Voc led to an enhanced power conversion efficiency. This power conversion efficiency was a 21% improvement from the standard cell to the most efficient loading (from 2.85% to 3.62%). The FF of all devices were within what would be expected for standard devices made from P3HT with annealing time of 3 min. as shown in Table 3.3. The J-V (current-voltage) measurements was shown in Figure 3.13

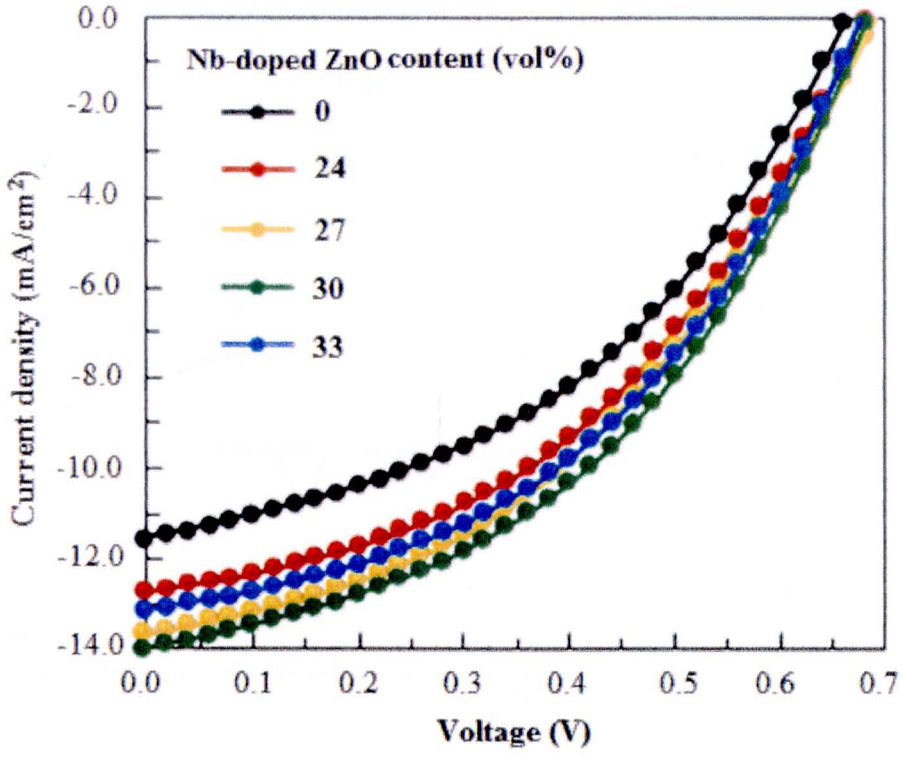

Figure 3.13 The J-V curves of P3HT:PCBM:Nb-doped ZnO photovoltaic cells measured in the ambient atmosphere with 120 mW/cm^2 white-light irradiation.

Figure 3.14 shows external quantum efficiency (EQE) spectra of the photovoltaic devices with and without Nb-doped ZnO nanoparticles. The EQE measurements show an increase in photon collection, and thus photocurrent, across all wavelengths absorbed. A maximum over 50% in the region around 510 nm can be seen for the photovoltaic cell with Nb-doped ZnO nanoparticles. Contributions to the photocurrent from both P3HT (400–700 nm) and PCBM (300–400 nm) are evident. The park in the EQE spectra at 375 nm resulted from absorption of Nb-doped ZnO nanoparticles and the hole transfer to the P3HT [57–58], corresponding to the probable band gap of the Nb-doped ZnO nanoparticles. The Nb-doped ZnO nanoparticles absorbed the light of wavelength shorter than 375 nm, as shown in the

Figure 3.15. While the device without Nb-doped ZnO nanoparticles of 480 nm length showed the EQE of 49%. In the region of wavelength shorter than 425 nm, the EQE values of the photovoltaic cells without Nb-doped ZnO nanoparticles were quenched sharply, in comparison with that of the photovoltaic cell with Nb-doped ZnO nanoparticles. This result was consistent with the result from the current-voltage characteristics. Therefore, it is considered that the functions of the Nb-doped ZnO nanoparticles in the photovoltaic devices are mainly to act as an electron collector and transporter.

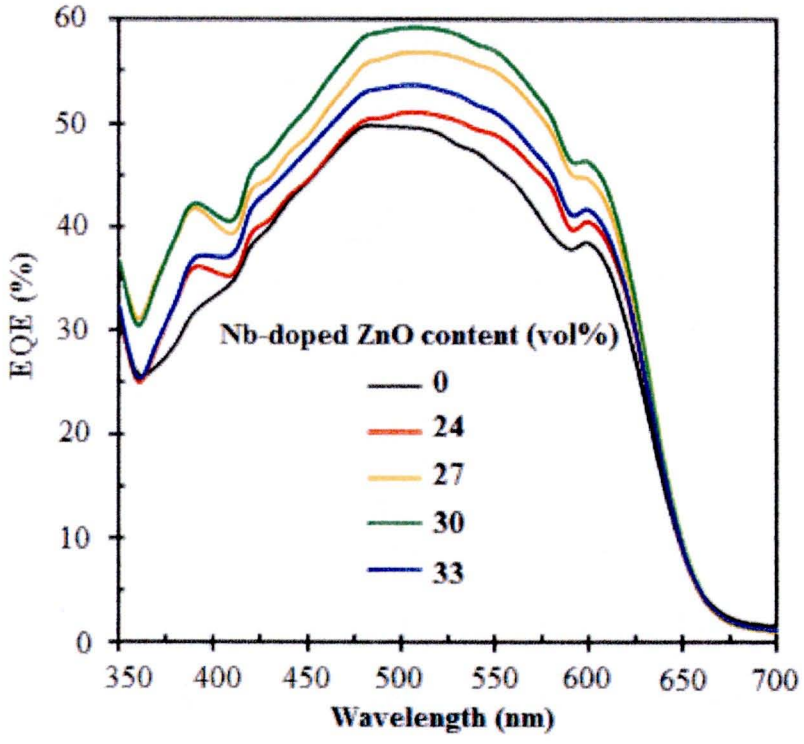

Figure 3.14 EQE spectra of the device fabricated using BHJ films with 3.00 mol% Nb-doped ZnO concentrations of 24, 27, 30, and 33 vol%.

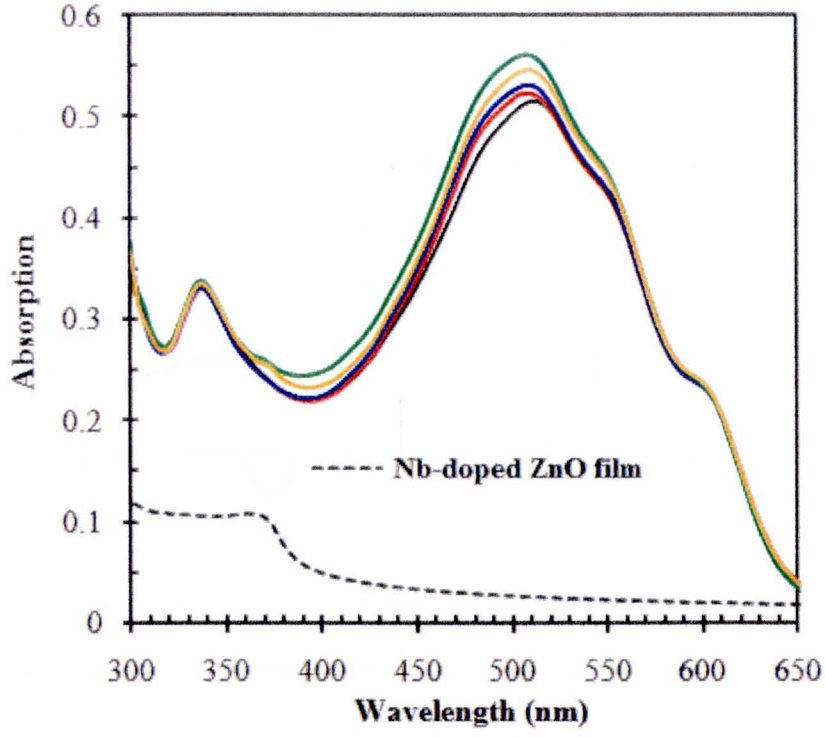

Figure 3.15 Absorption spectra of P3HT:PCBM:Nb-doped ZnO films at various concentrations of Nb-doped ZnO solution blended into the P3HT:PCBM active layer.

Table 3.3 Solar cell parameters.

3.00 mol% Nb-doped ZnO content (vol%)	**V_{oc} (V)**	**I_{SC} (mA/cm^2)**	**FF**	**η (%)**
0	0.663	11.5	0.429	2.85
24	0.682	12.7	0.429	3.24
27	0.689	13.6	0.416	3.39
30	0.682	13.9	0.437	3.62
33	0.676	13.1	0.443	3.42

One possible explanation is that the Nb-doped ZnO particles act as scatterers within the active layer of the device. This scattering effect could lead to better absorption via optical confinement within the device. Competing scattering effects (scattering within the active layer and scattering out of the active layer) could explain the current drop off from 30 to 33 vol% devices, with reflection out of the device beginning to dominate. Charge transport could also be changed significantly with high nanoparticles' content, leading to suboptimal device characteristics (improved or degraded charge carrier mobility can affect the overall charge balance of the device). This could also be the reason that niobium doped particles have a positive effect on the device as opposed to the negative effect evidenced by the ZnO particles as the niobium could have an effect on how the nanoparticles integrate into the BHJ film (via band structure changes). The slight increase in V_{OC} can be attributed to the change in band alignment caused by the introduction of the Nb-doped ZnO nanoparticles, a similar effect is seen with undoped ZnO nanoparticles. Scattering effects could be enhanced by the smaller particle sizes that are created by increased niobium doping (effectively increasing the scattering cross section).

Devices with just 1-butanol in the appropriate concentrations were also made in order to determine the effect of the solvent on device performance (Figure 3.16). No substantial effect was observed.

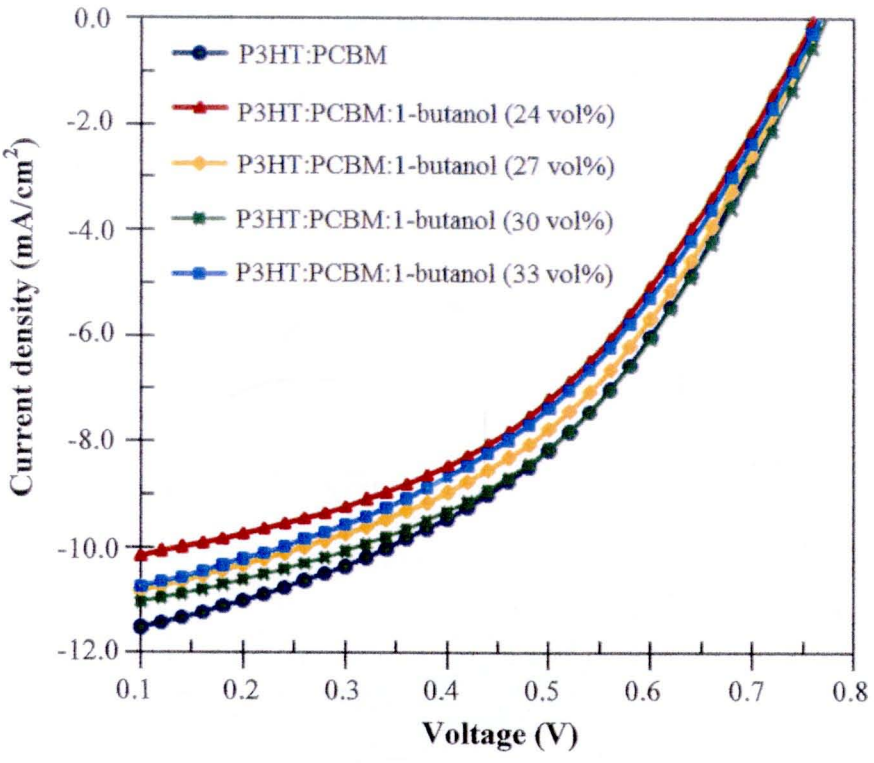

Figure 3.16 The J-V curves of P3HT:PCBM:1-butanol photovoltaic cells measured in the ambient atmosphere with 120 mW/cm^2 white-light irradiation.

3.4.2 The effect of niobium doping on composite solar cells using the 3.00 mol% Nb-doped ZnO nanoparticles and the use of 1, 3, 5-trichlorobenzene (TCB) as co-solvent for enhancing nanostructured P3HT:PCBM: Nb-doped ZnO layer.

The J-V measurements are shown in Figure 3.17. Nb-doped ZnO particles synthesized with 3.00 mol% concentration of niobium were then used to investigate the effect of nanoparticles on the photovoltaic characteristics of devices. From the data summarized in Table 3.4, there is a small increase in open circuit voltage (V_{OC}) for Nb-doped ZnO doped devices. The Nb-doped ZnO solution-blended P3HT:PCBM films exhibited higher values of J_{SC} with the maximum value of 9.02 mA cm^{-2}

obtained with annealing time of 7 min. (8.94 mA/cm^2 for the unmodified device). The increased J_{SC} and V_{OC} led to the enhanced power conversion efficiency (η). This power conversion efficiency was a 16.4% improvement from the standard cell to the most efficient loading (from 2.90% to 3.47%).

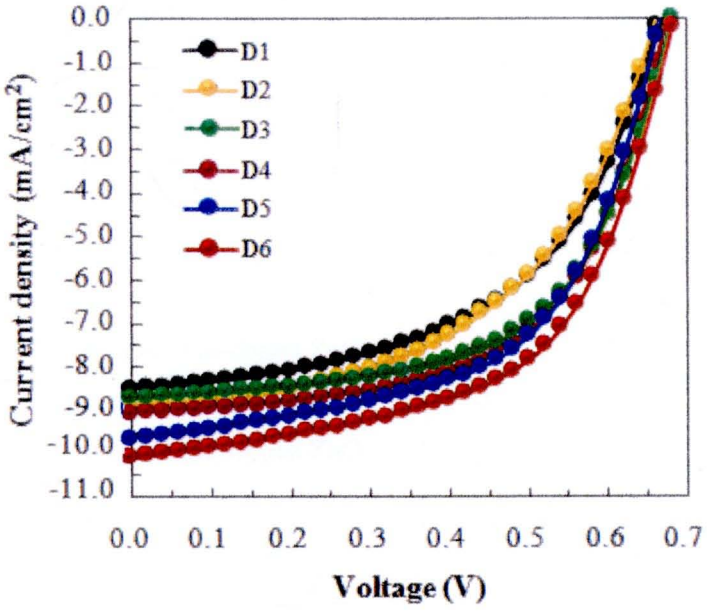

Figure 3.17 J-V characteristics of P3HT:PCBM and P3HT:PCBM:3.00 mol% Nb-doped ZnO bulk-hetero junction solar cells blends (both with and without added TCB) annealed for 5 and 7 min.

Table 3.4 Solar cells characteristics of P3HT: PCBM and P3HT:PCBM:3.00 mol% Nb-doped ZnO bulk-hetero junction solar cells blends (both with and without added TCB) annealed for 5 and 7 min.

Samples	V_{oc} (V)	I_{SC} (mA/cm^2)	FF	η (%)
D1: P3HT:PCBM (CB-5min)	0.663	8.49	0.529	2.89
D2: P3HT:PCBM (CB-7min)	0.660	8.94	0.506	2.90
D3: P3HT:PCBM:3.00 mol% Nb-doped ZnO (CB-5min)	0.680	8.72	0.588	3.38
D4: P3HT:PCBM:3.00 mol% Nb-doped ZnO (CB-7min)	0.674	9.02	0.588	3.47
D5: P3HT:PCBM:3.00 mol% Nb-doped ZnO (CB+TCB-5min)	0.665	9.65	0.566	3.53
D6: P3HT:PCBM:3.00 mol% Nb-doped ZnO (CB+TCB-7min)	0.682	10.10	0.567	3.79

The effect of TCB as co-solvent in the polymer solution on the performance of the devices was also investigated as shown in Figure 3.17. The best performance, with a short-circuit current density J_{SC} =10.1 mA/cm^2 , a fill factor *FF*=0.567, an open-circuit voltage V_{OC} = 0.682V and a resulting efficiency of 3.79%, could be reached for a cell blended with 3.00 mol% Nb-doped ZnO solution and annealed at 150°C for 7 min with a TCB concentration of 3.5 mg/ml. This yielded an 11% improvement over the devices obtained under the same conditions but without the inclusion of TCB. The *FF* of all devices was within what would be expected for standard devices made with this P3HT and annealed for 5 and 7 min.

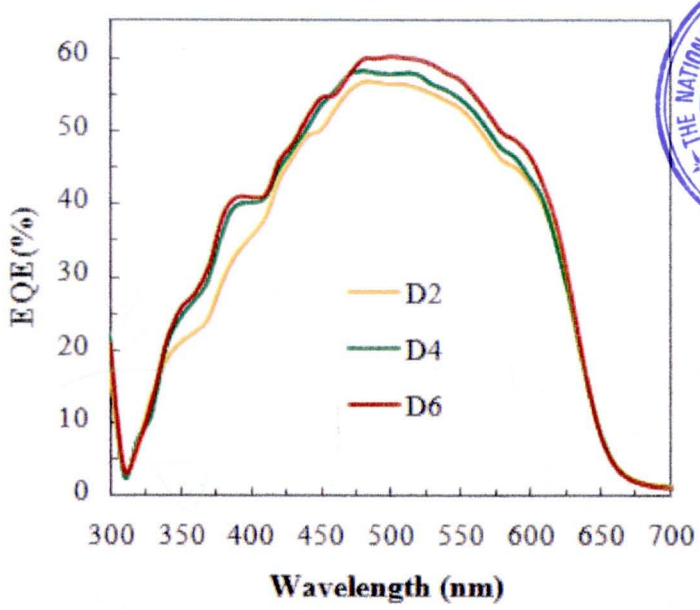

Figure 3.18 EQE spectra of P3HT:PCBM and P3HT:PCBM:3.00 mol%Nb-doped ZnO bulk-hetero junction solar cells blends (both with and without added TCB) annealed for 7 min.

The EQE measurements show an increase in photon collection, and thus photocurrent, across all wavelengths absorbed as seen in Figure 3.18. There is a prominent increase at 385 nm, corresponding to the probable band gap of 3.2 eV of ZnO. The morphology of P3HT:PCBM:3.00 mol%Nb-doped ZnO layers from spin-coated CB solution and mixed solution (CB and TCB) after annealing at 150 °C for 7 min., have been studied using AFM.

AFM topography images indicate the smoother film surface of the P3HT:PCBM:3.00 mol% Nb-doped ZnO when TCB was used as the co-solvent in the blend, as shown in Figure 3.19 Film as prepared from CB+TCB, the surface is rather smooth with r.m.s. roughness of 0.854 nm, while the film prepared from CB shows r.m.s. ~ 1.794 nm. The surface of film was smoother with the addition of TCB at 3.5

mg/ml, which in turn improved the organic/cathode contact. The power conversion efficiency of such fabricated solar cells was higher than that of cells formed without TCB solvent.

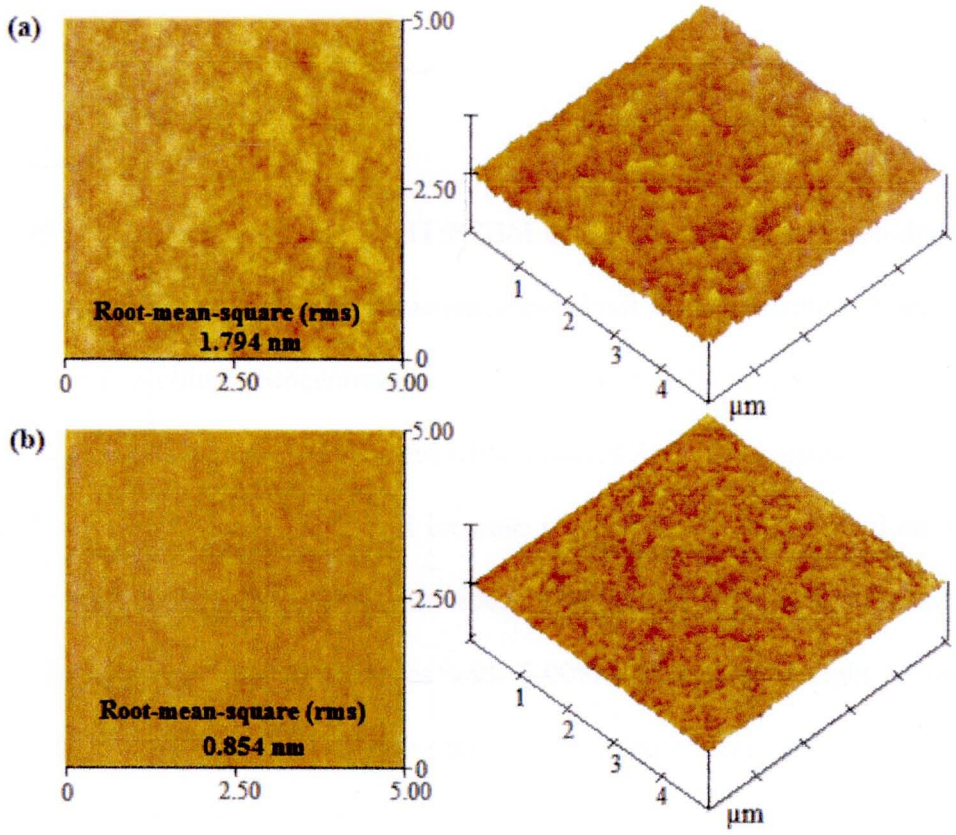

Figure 3.19 AFM images of P3HT:PCBM:3.00 mol% Nb-doped ZnO spin-coated from (a) CB and (b) CB+TCB annealed for 7 min.

One possible explanation is that the Nb-doped ZnO particles act as scatterers within the active layer of the device. This scattering effect could lead to better absorption via optical confinement within the device. Charge transport could also be changed significantly with nanoparticles' content, leading to suboptimal device characteristics (improved or degraded charge carrier mobility can affect the overall charge balance of the device). This could also be the reason that niobium doped particles have a positive effect on the device as opposed to the negative effect

evidenced by the ZnO particles as the niobium could have an effect on how the nanoparticles integrate into the BHJ film. The slight increase in V_{OC} can be attributed to the change in band alignment caused by the introduction of the Nb-doped ZnO nanoparticles [59].

3.5 Conclusions

BHJ solar cells utilizing P3HT:PCBM composite loaded with Nb-doped zinc oxide nanoparticles produced by flame spray pyrolysis were fabricated. Nanoparticles with different niobium concentrations were compared, along with devices without Nb-doped zinc oxide nanoparticles and with undoped ZnO nanoparticles. It was found that niobium doping leads to a slight increase in open circuit voltage and an increase in short circuit current that scales with niobium concentration. Additional comparison was made between the nanoparticles with 3.00% niobium by weight to unloaded devices. These also showed a similar open circuit voltage increase and an increase in current that scales with Nb-doped zinc oxide nanoparticle concentration to 30% by volume and drops off at 33% Nb-doped zinc oxide by volume. The effect of co-solvent (1, 3, 5-trichlorobenzene; TCB) in chlorobenzene in the polymer solution was also investigated on the morphology and performance of a P3HT:PCBM and P3HT:PCBM:Nb-doped ZnO bulk-heterojunction solar cells. The device efficiency was improved due to a good quality of the thin film nanostructure and annealing time.

REFERENCES

1. Halls J.J.M., Walsh C.A., Greenham N.C., Marseglia E.A., Friend R.H, Moratti S.C., Holmes A.B., Efficient photodiodes from interpenetrating polymer networks, *Nature*, 1995, **376**, 498–500.

2. Veenstra S.C., Verhees W.J.H., Kroon J.M., Koetse M.M., Sweelssen J., Bastiaansen J.J.A.M., Schoo H.F.M., Yang X., Alexeev A., Loos J., Schubert U.S., Wienk M.M., Photovoltaic Properties of a Conjugated Polymer Blend of MDMO-PPV and PCNEPV, *Chem. Mater.*, 2004, **16**, 2503–2508.

3. Yu G., Heeger A.J., Charge separation and photovoltaic conversion in polymer composites with internal donor/acceptor heterojunction, *J. Appl. Phys.*, 1995, **78**, 4510–4515.

4. Yu G., Gao J., Hummelen J.C., Wudl F., Heeger A.J., Polymer photovoltaic cells: enhanced efficiencies via a network of internal donor-acceptor heterojunctions, *Science*, 1995, **270**, 1789–1791.

5. Svensson M., Zhang F., Veenstra S.C., Verhees W.J.H., Hummelen J.C., Kroon J.M., Inganas O., Andersson M.R., High performance polymer solar cells of an alternating polyfluorene copolymer and a fullerene derivative, *Adv. Mater.*, 2003, **15**, 988–991.

6. Kwong C Y., Djurisic A.B., Chui P.C., Cheng K.W., Chan W.K., Influence of solvent on film morphology and device performance of poly(3-hexylthiophene):TiO_2 nanocomposite solar cells, *Chem. Phys. Lett.*, 2004, **384**, 372–375.

7. Beek W.J.E., Wienk M.M., Janssen R.A.J., Efficient hybrid solar cells from zinc oxide and a conjugated polymer, *Adv. Mater.*, 2004, **16**, 1009–1013.

8. Huynh W.U., Dittmer J.J., Alivisatos A.P., Hybrid Nanorod-Polymer Solar Cells, *Science,* 2002, **295**, 2425–2427.

9. Beek W. J. E., Wienk M.M., Janssen R.A. J., Hybrid polymer solar cells based on zinc oxide, *Mater. Chem.,* 2005, **15**, 2985–2988.

10. Sun B., Marx E., Greenham N.C., Photovoltaic devices using blends of branched CdSe nanoparticles and conjugated polymers, *Nano Lett.*, 2003, **3**, 961–963.

11. Olson D.C., Shaheen S.E., White M.S.A., Band-Offset Engineering for Enhanced Open-Circuit Voltage in Polymer-Oxide Hybrid Solar Cells, *Adv. Funct. Mater.,* 2007, **17**, 264–269.

12. Beek W.J.E., Wienk M.M., Janssen R.A J., Hybrid Solar Cells from Regioregular Polythiophene and ZnO Nanoparticles, *Adv. Funct. Mater.,* 2006, **16**, 1112–1116.

13. Kim K., Liu J., Namboothiry M.A.G., Carroll D. L., Roles of donor and acceptor nanodomains in 6% efficient thermally annealed polymer photovoltaics, *Appl. Phys. Lett.*, 2007, 90, 163511–163513.

14. Lin J.M., Zhang Y.Z., Ye Z.Z., Gu X.Q., Pan X.H., Yang Y.F., Lu J.G., He H.P., Zhao B.H., Nb-doped ZnO transparent conducting films fabricated by pulsed laser deposition, *Appl. Surf. Sci.*, 2009, **255**, 6460–6463.

15. Wang H., Xie C., Zhang W., Cai S., Gui Z., Comparison of dye degradation efficiency using ZnO powders with various size scales, *J. Hazard. Mater.*, 2007, **141**, 645–652.

16. Teleki A., Bjelobrk N., Pratsinis S.E., Flame- made Nb- and Cu-doped TiO_2 sensors for CO and ethanol, *Sens. Actuators B*: Chem., 2008, **130**, 449–457.

17. http://www.unep.org/geo/yearbook. (December, 12 2010)

18. http://www.meto.gov.uk. (December, 12 2010).

19. Chapin D.M., Fuller C.S., Pearson G.L., A new silicon p-n junction photocell for con-verting solar radiation into electrical power, *J. Appl. Phys,* 1954, **25**, 676–677.

20. Green M.A., Emery K., King D.L., Igari S., Warta W., Solar cell efficiency tables (version 25), *Prog. Photovoltaics,* 2005, **13**, 49–56.

21. Shockley W., Queisser H.J., Detailed balance limit of efficiency of p-n junction solar cells, *J. Appl. Phys.,* 1961, **32**, 510–519.

22. Shaheen S.E., Radspinner R., Peyghambarian N., Jabbour G.E., Fabrication of bulk heterojunction plastic solar cells by screen printing, *Appl. Phys. Lett.*, 2001, **79**, 2996–2998.

23. Gustafsson G., Cao Y., Treacy G.M., Klavetter F., Colaneri N., Heeger A.J., Flexible light-emitting-diodes made from soluble conducting polymers, *Nature*, 1992, **357**, 477–479.

24. Scharber M.C., Muhlbacher D., Koppe M., Denk P., Waldauf C., Heeger A.J., Brabec C.J., Design rules for donors in bulk-heterojunction solar cells-towards 10% energy-conversion efficiency, *Adv. Mater.,* 2006, **18**, 789.

25. Meissner D., Plastic Solar Cells, *Photon*, 1999, **2**, 34–37.

26. Brabec C.J., Padinger F., Sariciftci N.S., Hummelen J.C., Photovoltaic properties of conjugated polymer/methanofullerene composites embedded in a polystyrene matrix, *J. Appl. Phys.*, 1999, **85**, 6866–6872.

27. Padinger F., Brabec C.J., Fromherz T., Hummelen J.C., Sariciftci N.S., Fabrication of large area photovoltaic devices containing various blends of polymer and fullerene derivatives by using the doctor blade technique, *Opto-Electron. Rev.*, 2000, **8**, 280–283.

28. Brabec C.J., Padinger F., Hummelen J.C., Janssen R.A.J., Sariciftci N.S., Realization of large area flexible fullerene-conjugated polymer photocells: a route to plastic solar cells, *Synthetic. Met.*, 1999, **102**, 861–0864.

29. Crispin X., Marciniak S., Osikowicz W., Zotti G., A. van der Gon W.D., Louwet F., Fahlman M., Groenendaal L., De Schryver F., Salaneck W.R., Conductivity, morphol-ogy, interfacial chemistry, and stability of poly(3,4-ethylene dioxythiophene)-poly(styrene sulfonate): A photoelectron spectroscopy study, *J. Polym. Sci. Pol. Phys.*, 2003, **41**, 2561–2583.

30. Ouyang B.Y., Chi C.W., Chen F.C., Xi Q.F., Yang Y., High-conductivity poly (3,4-ethylenedioxythiophene):poly(styrene sulfonate) film and its application in polymer optoelectronic devices, *Adv. Funct. Mater.*, 2005, **15**, 203–208.

31. Huang J.S., Miller P.F., Wilson J.S., A. deMello J., J. deMello C., Bradley D.D.C., Investigation of the effects of doping and post-deposition

treatments on the conductivity, morphology, and work function of poly (3,4 ethylenedioxythiophene)/poly (styrene sulfonate) films, *Adv. Funct. Mater.*, 2005, **15**, 290–296.

32. Schilinsky P., Waldauf C., Brabec C.J., Recombination and loss analysis in polythiophene based bulk heterojunction photodetectors, *Appl. Phys. Lett.*, 2002, **81**, 3885–3887.

33. Dyakonov V., Electrical aspects of operation of polymer-fullerene solar cells, *Thin Solid Films*, 2004, **451-52**, 493–497.

34. Riedel I., Parisi J., Dyakonov V., Lutsen L., Vanderzande D., Hummelen J.C., Effect of temperature and illumination on the electrical characteristics of polymer-fullerene bulk- heterojunction solar cells, *Adv. Funct. Mater.*, 2004, **14**, 38–44.

35. Duren van J.K.J., Yang X.N., Loos J., Bulle-Lieuwma C.W.T., Sieval A.B., Hummelen J.C., Janssen R.A J., Relating the morphology of poly(p-phenylene viny-lene)/methanofullerene blends to solar-cell performance, *Adv. Funct. Mater.*, 2004, **14**, 425–434.

36. Hoppe H., Arnold N., Sariciftci N.S., Meissner D., Modeling the optical absorption within conjugated polymer/fullerene-based bulk-heterojunction organic solar cells, *Sol. Energ. Mater. Sol. C.*, 2003, **80**, 105–113.

37. Shaheen S.E., Brabec C.J., Sariciftci N.S., Padinger F., Fromherz T., Hummelen J.C., 2.5% efficient organic plastic solar cells, *Appl. Phys. Lett.*, 2001, **78**, 841–843.

38. Trupke T., Würfel T., Uhlendorf I., Dependence of the photocurrent conversion efficiency of dye-sensitized solar cells on the incident light intensity, *J. Phys. Chem. B,* 2000, **104**, 11484–11488.

39. Kroon J.M., Wienk M.M., Verhees W.J.H., Hummelen J.C., Accurate efficiency determination and stability studies of conjugated polymer/fullerene solar cells, Thin Solid Films, *Thin Solid Films,* 2002, **403–404**, 223–228.

40. Goliber T.E., Perlstein J.H., Analysis of photogeneration in a doped polymer system interms of a kinetic-model for electric-field-assisted dissociation of charge-transfer states, *J. Chem. Phys.,* 1984, **80**, 4162–4167.

41. Hummelen J.C., Knight B.W., Lepeq F., Wudl F., Yao J., Wilkins C.L., Preparation and characterization of fulleroid and methanofullerene derivatives, *J. Org. Chem.,* 1995, **60**, 532–538.

42. Tang C.W., Two-layer organic photovoltaic cell, *Appl. Phys. Lett.*, 1986, **48**, 183–185.

43. Granström M. Petritsch, K., Arias A.C., Lux A., Andersson M.R., Friend R.H., Laminated fabrication of polymeric photovoltaic diodes, *Nature*, 1998, **395**, 257–260.

44. Padinger F., Rittberger R.S., Sariciftci N.S., Effects of postproduction treatment on plas-tic solar cells, *Adv. Funct. Mater.*, 2003, **13**, 85–88.

45. Brabec C.J., Organic photovoltaics: technology and market, *Sol. Energ. Mater. Sol. C.,* 2004, **83**, 273–292.

46. Kim Y., Choulis S.A., Nelson J., Bradley D.D.C., Cook S., Durrant J.R., Device annealing effect in organic solar cells with blends of

regioregular poly(3-hexylthiophene) and soluble fullerene, *Appl. Phys. Lett.* 2005, **86**, 063502–063504.

47. Li G., Shrotriya V., Huang J., Yao Y., Moriarty T., Emery K. Yang Y. High-efficiency solution processable polymer photovoltaic cells by self-organization of polymer blends. *Nat. Mater.*, 2005, **4**, 864–868.

48. Kim Y., Cook S., Tuladhar S.M., Choulis S.A., Nelson J., Durrant J.R., Bradley D.D.C., Giles M., McCulloch I., Ha C.-S., Ree M., A strong regioregularity effect in self-organizing conjugated polymer films and high-efficiency polythiophene:fullerene solar cells, *Nat. Mater.*, 2006, **5**, 197–203.

49. Irwin M.D., Buchholz D.B., Hains A.W., Chang R.P.H., Marks T.J., p-type semiconducting nickel oxide as an efficiency-enhancing anode interfacial layer in polymer bulk-heterojunction solar cells, *P. Natl. Acad. Sci.*, 2008, **105**, 2783–2787.

50. Chang M.Y., Chen Y.F., Tsai Y.S., Chi K.M., Institute of electro-optical engineering and department of photonics, *J. Electrochem. Soc., 2009,* **156,** 234–237.

51. Takanezawa K., Hirota K., Wei Q.S., Tajima K., Hashimoto K., Efficient charge collection with ZnO nanorod array in hybrid photovoltaic devices, *J. Phys. Chem. C,* 2007, **111**, 7218–7223.

52. Beek W.J.E., Wienk M.M., Kemerink M., Yang X., Janssen A.J., Hybrid zinc oxide conjugated polymer bulk heterojunction solar cells, *J. Phys. Chem. B,* 2005, **109**, 9505–9516.

53. Wang M., Wang X., P3HT/ZnO bulk-heterojunction solar cell sensitized by a perylene derivative, *Sol. Energ. Mater. Sol. C.*, 2008, **92**, 766–771.

54. Greenham N.C., Peng X., Alivisatos A.P, Charge separation and transport in conjugated-polymer/semiconductor-nanocrystal composites studied by photoluminescence quenching and photoconductivity, *Phys. Rev. B.*, 1996, **54**, 628–237.

55. Kim S.H., Kim H.H., lee K., Lee W., Ma X., Gong A., Heeger J., New architecture for high-efficiency polymer photovoltaic cells using solution-based titanium oxides as an optical spacer, *Adv. Mater.*, 2006, **18**, 572–576.

56. Law M., Greene L.E., Johnson J.C., Saykally R., Yang P.D., Nanowire dye-sensitized solar cells, *Nat. Mater.*, 2005, **4**, 455–459.

57. Olson, D.C., Piris, J., Collins, R.T., Shaheen, S.E., Ginley, D.S. Hybrid photovoltaic devices of polymer and ZnO nanofiber composites. *Thin Solid Films*, 2006, **496**, 26–29.

58. Unalan H.E., Hiralal P., Kuo D., Parekh B., Amaratunga G., Chhowalla M., Flexible organic photovoltaics from zinc oxide nanowires grown on transparent and conducting single-walled carbon nanotube films, *J. Mater. Chem.*, 2008, **18**, 5909–5912.

59. Kaidashev E.M., Lorenz M., Wenckstern V.H., Rahm A., Semmelhack H.C., Han K.H., Benndorf G., Bundesmann C., Hochmuth H., Grundmann M., High electron mobility of epitaxial ZnO thin films on c-plane sapphire grown by multi-step pulsed laser deposition, *Appl. Phys. Lett.*, 2003, **82**, 3901–3903.